Publication Year	2024
Acceptance in OA	2024-01-26T10:41:04Z
Title	Multi-technique investigation of silicon nitride/aluminum membranes as optical blocking filters for high-energy space missions
Authors	SCIORTINO, Luisa, BARBERA, Marco, FERRUGGIA BONURA, Salvatore, TODARO, Michela, PUCCIO, ELENA, D'ANCA, FABIO, Cicero, Ugo Lo, Törmä, Pekka T., Magnano, Elena, Nappini, Silvia, Píš, Igor, Perinati, Emanuele, Diebold, Sebastian, Guzman, Alejandro, Tenzer, Chris, Buscarino, Gianpiero, Gollwitzer, Christian, Handick, Evelyn, Krumrey, Michael, Laubis, Christian, CANDIA, Roberto, VARISCO, Salvatore
Publisher's version (DOI)	10.1117/1.JATIS.10.1.018002
Handle	http://hdl.handle.net/20.500.12386/34631
Journal	JOURNAL OF ASTRONOMICAL TELESCOPES, INSTRUMENTS, AND SYSTEMS
Volume	10

JATIS Journal of Astronomical Telescopes, Instruments, and Systems

RESEARCH PAPER

Multi-technique investigation of silicon nitride/aluminum membranes as optical blocking filters for high-energy space missions

Luisa Sciortino,[a,b,*] Marco Barbera,[a,b] Salvatore Ferruggia Bonura,[b] Michela Todaro,[a,b] Elena Puccio,[a,b] Fabio D'Anca,[a,b] Ugo Lo Cicero,[a,b] Pekka T. Törmä,[c] Elena Magnano,[d,e] Silvia Nappini,[d] Igor Píš,[d] Emanuele Perinati,[f] Sebastian Diebold,[f] Alejandro Guzman,[f] Chris Tenzer,[f] Gianpiero Buscarino,[b] Christian Gollwitzer,[g] Evelyn Handick,[g] Michael Krumrey,[g] Christian Laubis,[g] Roberto Candia,[a] and Salvatore Varisco[a]

[a]Istituto Nazionale di Astrofisica (INAF), Osservatorio Astronomico di Palermo, Palermo, Italy
[b]Università degli Studi di Palermo, Dipartimento di Fisica e Chimica - Emilio Segrè, Palermo, Italy
[c]Ametek Finland Ltd., Espoo, Finland
[d]IOM-CNR, Laboratorio TASC, Trieste, Italy
[e]University of Johannesburg, Department of Physics, Auckland Park, South Africa
[f]Eberhard Karls Universität Tübingen, Institut für Astronomie und Astrophysik, Tübingen, Germany
[g]Physikalisch-Technische Bundesanstalt, Berlin, Germany

ABSTRACT. X-ray detectors for space astrophysics missions are susceptible to noise caused by photons with energies outside the operating energy range; for this reason, efficient external optical blocking filters are required to shield the detector from the out-of-band radiation. These filters play a crucial role in meeting the scientific requirements of the X-ray detectors, and their proper operation over the life of the mission is essential for the success of the experimental activity. We studied thin sandwich membranes made of silicon nitride and aluminum as optical blocking filters for high-energy detectors in space missions. Here, we report the results of a multi-technique characterization of SiN membranes with thicknesses in the range from 40 nm to 145 nm coated with few tens of nanometers of aluminum on both sides. In particular, we have measured the X-ray transmission at synchrotron radiation beamlines, the rejection of ultraviolet, visible, and near-infrared radiation, the amount of native oxide on the aluminum surfaces by X-ray photoelectron spectroscopy, the morphology of the sample surfaces by atomic force microscopy, and the aging effects under proton irradiation.

 [DOI: 10.1117/1.JATIS.10.1.018002]

Keywords: optical blocking filter; silicon nitride; spectroscopic characterization; aluminum; proton irradiation

Paper 23126G received Oct. 15, 2023; revised Dec. 28, 2023; accepted Jan. 5, 2024; published Jan. 24, 2024.

1 Introduction

High-sensitivity X-ray detectors are affected by out-of-range radiation [microwave, infrared (IR), visible (VIS), and ultraviolet (UV)], which can deteriorate their performance. The presence of filters to shield the detectors is thus necessary for the correct operation of the detector, yet their X-ray transparency must be maximized to guarantee a high detection efficiency.

*Address all correspondence to Luisa Sciortino, luisa.sciortino@inaf.it

Charge-coupled devices, silicon drift detectors, and depleted p-channel field effect transistor arrays, as baselined for the wide field imager[1] (WFI) instrument of the Athena mission, are sensitive to UV and visible photons with energy larger than the Si band gap. If these photons hit such a detector, electron-hole pairs are formed, which add to those generated by the X-ray photon, causing a spectral resolution degradation, and a shift of the energy scale by a few eV. An optical blocking filter (OBF) is thus required to remove UV and visible radiation which is typically brighter than X-rays in most astrophysical sources.[2] OBFs are particularly important for experiments observing the EUV and X-ray emission from the chromosphere and solar corona, in this case the much brighter UV/VIS emission from the photosphere must be fully blocked. A few such examples include the X-ray telescope experiment[3] on Hinode, the extreme ultraviolet imaging telescope[4] experiment on Solar and Heliospheric Observatory, and the extreme ultraviolet imager experiment[5] on Solar Orbiter.

Filters are usually made of a shielding layer, usually a low-Z metal such as aluminum for keeping a low X-ray attenuation, and a supporting membrane, which is needed because the low thickness needed to allow for limiting the X-ray attenuation does not ensure sufficient mechanical strength.

Silicon nitride is a good candidate as a filter support material since both silicon and nitrogen are low-Z chemical elements, silicon nitride (SiN) is known to be thermodynamically stable [6,7] and, additionally, the related technological processes are well developed because this compound is extensively employed in the fabrication of integrated circuits. The most used materials to fabricate filters for X-rays missions are polymers, in particular polyimide, because their excellent mechanical properties. However, this class of materials contains a very large amount of carbon resulting in high absorption around the C K-edge.

Filters based on SiN are in general less transparent than most of used polymeric thin films like polyimide as it can be seen in Fig. 1 (calculated curves). To be competitive with polyimide the SiN membrane thickness shall be at least half the thickness of the polymer. In addition, the Si L edge at around 100 eV is quite pronounced significantly reducing the transmission up to the N K edge at around 400 eV.

On the other hand, being SiN carbon free, it may have niche applications when high transparency is required around the C K-edge region.

Performing a spectroscopic characterization of sandwiches composed of silicon nitride and aluminum is a fundamental step for designing filters with these materials; since their spectroscopic properties strongly depend both on their intrinsic properties and on their thickness and morphology.[8]

In this paper, we show a multi-technique investigation [UV-VIS-NIR spectroscopy, X-ray photoelectron spectroscopy (XPS), X-ray transmission spectroscopy, and atomic force microscopy (AFM)] of Al-coated ultra-thin silicon nitride membranes. Furthermore, a selection of these

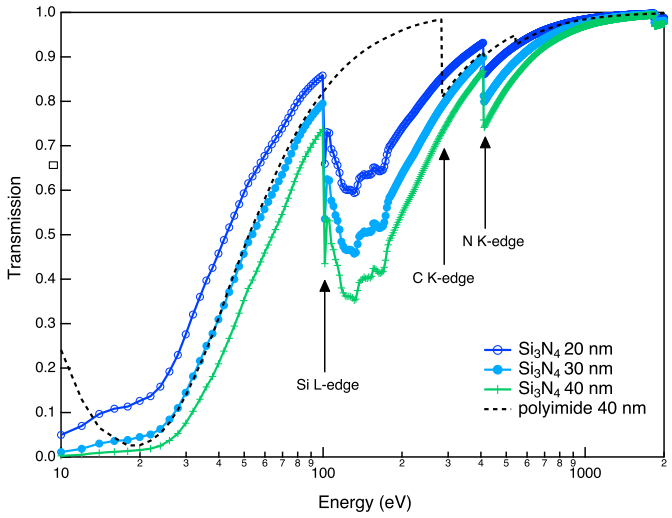

Fig. 1 Comparison of the calculated transmission of 40 nm of polyimide (black dashed line), 40 nm of Si_3N_4 (green solid line), 30 nm of Si_3N_4 (light blue solid line), and 20 nm of Si_3N_4 (dark blue solid line).

were irradiated with different proton doses, and then characterized by spectroscopy and AFM to assess any potential modifications in their properties. We measured the X-ray transmission of these materials and recovered the thicknesses of all the present layers by modeling. The analysis of X-ray photoelectron spectra allowed us to derive the thickness of the native aluminum oxide that reduces the nominal amount of metallic aluminum. We also studied these filter samples by UV/VIS/NIR spectroscopy to estimate the attenuation capability in this band, which is relevant in space when such filters are used to protect EUV/X-ray detectors from Sun light and out-of-band optical load from other astrophysical sources.

2 Materials and Methods

2.1 Samples

The membranes under investigation are made of silicon nitride, with aluminum coating applied on both surfaces. For reference a silicon nitride membrane without Al coating was also characterized. Some samples are supported by a mesh, consisting of a honeycomb structure with silicon bars 15 μm thick and with a width of 17 μm, and a pitch of 200 μm, resulting in more than 80% open area (OA). When the mesh is present, it is placed between the one aluminum layer and the silicon nitride membrane. All the investigated samples were mounted on a small size metal frame, the standard TO-8 package used in semiconductor industries.[9] The outer diameter of the cap is ~15 mm, the height ~8.5 mm and the clear aperture diameter hosting the thin membrane is 7 mm. An optical scan acquired using a photographic scanner EPSON Perfection V850 Pro in transmission and in reflection mode of a typical filter sample mounted on a TO-8 frame is reported in Fig. 2.

The SiN layers were fabricated by low-pressure chemical vapor deposition, whereas the silicon mesh was patterned using standard lithography and plasma etching. The aluminum is deposited by sputtering deposition as reported in a previous paper.[6] The main characteristics of the silicon nitride/aluminum membrane samples investigated in this paper are reported in Table 1. The aluminum amount is close to that corresponding to the baseline of the filters of both instruments of Athena.[10,11] The samples with self-standing membranes (first four rows) were used to investigate the properties of pristine materials from a spectroscopic point of view, while the samples with membranes supported by a silicon mesh were mostly used to probe the radiation hardness.

2.2 Proton Irradiation

1 MeV proton irradiation was performed at the Van der Graaf accelerator at the Johann Wolfgang Goethe-Universität Frankfurt am Main[12] on a few samples supported by silicon mesh (Table 2). The irradiations were performed with different fluences, reported in Table 2, relative to the total non-ionizing radiation qualification fluence (Q.F.) equal to $1.2 \cdot 10^{10}$ cm^{-2} (equivalent to $9.4 \cdot 10^{10}$ cm^{-2} 10 MeV protons) corresponding to the radiation dose the Athena mission will undergo over the nominal lifetime of 4 years.

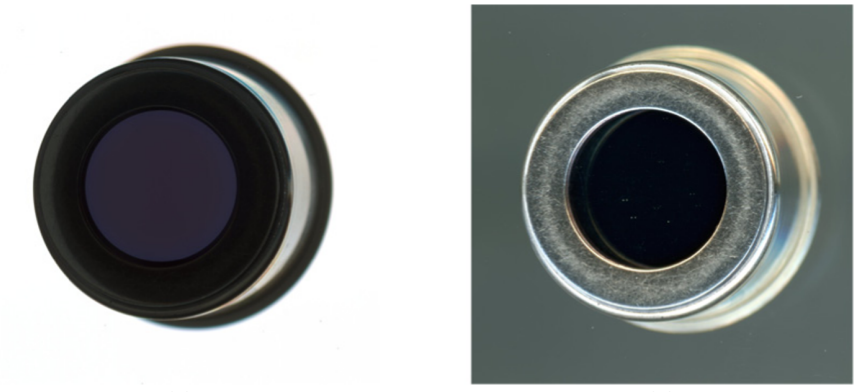

(a) (b)

Fig. 2 Optical scan in transmission (a) and in reflection mode (b) of a typical sample mounted on a TO-8 standard frame with 7 mm clear aperture diameter.

Table 1 Main characteristics of the silicon nitride/aluminum membrane samples investigated in this paper. Sample name, nominal thicknesses of aluminum and silicon nitride, OA, and mesh features are reported.

Sample name	Al (nm)	SiN (nm)	OA (%)	Mesh features (μm)
TO8-C1-1	2 × 10 ± 5%	145 ± 5%	100	—
TO8-C1-2	2 × 10 ± 5%	145 ± 5%	100	—
TO8-C2-1#2	2 × 10 ± 5%	40 ± 5%	100	—
TO8-C2-2#2	2 × 10 ± 5%	40 ± 5%	100	—
TO8-C2-6	2 × 15 ± 5%	40 ± 5%	82	Bar height 15
				Bar width 17
				Pitch size 200
TO8-C2-1	2 × 15 ± 5%	40 ± 5%	82	Bar height 15
				Bar width 17
				Pitch size 200
TO8-C2-5[a]	2 × 15 ± 5%	40 ± 5%	82	Bar height 15
				Bar width 17
				Pitch size 200
TO8-C2-2[a]	2 × 15 ± 5%	40 ± 5%	82	Bar height 15
				Bar width 17
				Pitch size 200
TO8-C2-3[a]	2 × 15 ± 5%	40 ± 5%	82	Bar height 15
				Bar width 17
				Pitch size 200
TO8-C2-31	0	40 ± 5%	82	Bar height 15
				Bar width 17
				Pitch size 200

[a]Samples irradiated with 1 MeV protons.

Table 2 List of samples supported by silicon mesh that have been irradiated with 1 MeV protons. The radiation dose is relative to Q.F. $= 1.2 \cdot 10^{10}$ cm^{-2}.

Sample name	Radiation dose (relative to Q.F.)
TO8-C2-5	1
TO8-C2-2	10
TO8-C2-3	100

2.3 X-ray Photoelectron Spectroscopy

XPS measurements were performed on four filter samples TO8-C1-2, TO8-C2-2#2, TO8-C2-6, and TO8-C2-2. As aforementioned, the sample TO8-C2-2 was irradiated with a fluence equal to 10 Q.F. while the TO8-C2-6 was pristine.

XPS measurements were performed at the BACH beamline of the Elettra synchrotron (Trieste, Italy), which is equipped with a hemispherical electron analyzer (VG Scienta

Table 3 Experimental conditions for the XPS data collection. The nominal kinetic energies of the outgoing electrons and the emission angle, α, with respect to surface normal are reported.

Sample name	KE of the photoemitted electron (eV)	α (deg)
TO8-C1-2	450, 550, and 750	0
TO8-C2-2#2	450, 550, and 750	0
TO8-C2-6	490, 800, and 1025	30
TO8-C2-2	450, 550, and 750	0

R3000) placed at 60° from the incident beam direction. The spot size of the beam was 0.300 mm × 0.15 mm (horizontal × vertical). The XPS spectra were recorded with linearly polarized synchrotron radiation, at a total instrumental resolution of 0.3 eV at 530 eV photon energy, and 0.5 eV at 1100 eV photon energy. We collected the Al 2p XPS spectra to estimate the amount of aluminum oxide, which is natively present on any aluminum surface. Binding energies of spectra were calibrated to Au $4f_{7/2}$ (84.0 eV) measured on an Au foil in electric contact with the samples.

Fits have been carried out using the X-ray photoelectron spectroscopy tools program package,[13] and a Shirley-type background, which is the typical function used to remove the background contribution caused by inelastic scattered electrons, was subtracted. Each peak is reproduced by a Gauss-Lorentzian sum function to approximate the Voigt profile. Al 2p XPS spectra were acquired in the experimental conditions reported in Table 3.

2.4 X-ray Transmission Measurements

X-ray transmission measurements were carried out at two X-ray beamlines of the Physikalisch-Technische Bundesanstalt at the BESSY II synchrotron radiation facility in Berlin – Germany: in the photon energy range from 50 to 1800 eV at the PTB soft X-ray beamline[14] and from 1750 to 3600 eV at the PTB Four-Crystal Monochromator (FCM) beamline.[15] The energy range investigated includes edges of the elements present in the filter: Al L-edges @73 eV and @118 eV, Si L-edges @99 eV and @149 eV, N K-edge @402 eV, O K-edge @532 eV, Al K-edge @1560 eV and Si K-edge @1839 eV. The energy scans were done sequentially with the direct beam measured before and after the filter measurement to control for stability. Additionally, the signal measured with no beam on was subtracted from each measurement.

At the soft X-ray beamline, measurements were performed with a spectral resolving power better than 1000, the spot size was $\sim 1.2 \times 1.0$ mm^2 (vertical × horizontal). Data near the C K-edge were not acquired since in this energy range the signal is insufficient due to carbon contamination of the beamline optics. The X-ray transmission measurements were performed at the soft X-ray beamline using different energy steps, as reported in Table 4.

The samples were also measured at PTB FCM[15] beamline, where the measurements were performed with the InSb crystals in the monochromator, providing a spectral resolving power better than 4000. The spot size was $\sim 0.3 \times 0.3$ mm^2. Transmission spectra are recorded in the energy range 1750 to 3600 eV, using different energy steps, as reported in Table 5.

2.5 UV/VIS/NIR Transmission

UV/VIS/NIR transmission spectra were collected at room temperature in transmission geometry using the double-beam spectrometer PerkinElmer Lambda1050+ available at the laboratory of INAF/OAPA. Given the small clear aperture diameter of the TO-8, a suitable sample holder was realized *ad hoc* to ensure high repeatability in positioning sample filters and an open TO-8 frame to acquire the blank spectra at the start of each measurement session. The measurement parameters were optimized by repeating transmission measurements for each filter to increase the signal-to-noise ratio. Data were collected in the 190 to 2000 nm range using a 2 nm data pitch.

Table 4 X-ray transmission measurements parameters adopted at PTB soft X-ray beamline.

		Al L-edge	Si L-edge		N K-edge		O K-edge		Al K-edge	
Energy range (eV)	50 to 70	70 to 94	94 to 180	180 to 390	390 to 450	450 to 520	520 to 570	570 to 1550	1550 to 1700	1700 to 1800
Sample name	Energy step in each range (eV)									
TO8-C1-1	2	0.2	0.2	5	0.4	5	0.4	20	1	10
TO8-C2-6	2	0.2	0.2	5	0.4	5	0.4	20	1	10
TO8-C2-5	2	0.2	0.2	5	0.4	5	0.4	20	1	10
TO8-C2-2	2	2	0.2	5	0.4	5	10	20	10	10
TO8-C2-31	2	2	0.2	5	0.4	5	10	20	10	10

Table 5 X-ray transmission measurement parameters adopted at the PTB FCM beamline.

	Si K-edge			
Energy range (eV)	1750 to 1830	1830 to 1900	1900 to 2200	2200 to 3600
Sample name	Energy step in each range (eV)			
TO8-C1-1	10	1	10	50
TO8-C2-6	10	1	10	50
TO8-C2-5	10	1	10	50
TO8-C2-2	10	1	10	50
TO8-C2-31	10	1	10	50

2.6 Atomic Force Microscopy

AFM measurements are acquired in air using a Bruker FAST-SCAN microscope. The images are obtained in tapping mode by using FAST-SCAN probes with an apical radius of about 5 nm. Each AFM image has a pixel resolution comparable to the tip size and surface micro-roughness resolution down to ~5 nm. The roughness of the surface has been measured over large areas of 8 μm × 8 μm. Three different samples were measured; two of the measured samples are pristine, TO8-C2-1 and TO8-C2-6, and one has been irradiated with 100 times the QF, TO8-C2-3.

3 Results and Discussion

All the Al 2p XPS spectra shown in Fig. 3 are composed of two main signals: a major contribution at higher binding energy attributed to the Al^{3+} (oxidized aluminum) component and a minor signal at lower energy assigned to the Al^0 component (metal aluminum). For the Al^0 is possible to resolve the doublet due to the spin-orbit coupling which corresponds to the two possible states having distinguishable binding energies, attributed to $2p_{1/2}$ and $2p_{3/2}$ Al peaks.[16]

Figure 3 shows that as the kinetic energy (KE) of the ejected electrons increases, the relative contribution of metallic aluminum increases with respect to the aluminum oxide. As the KE increases, the investigated thickness is larger, as the effective attenuation length (EAL) of the photoemitted electrons increases with the photon energy, thus more signal is detected from the deep metallic aluminum substrate with respect to the superficial oxide layer.

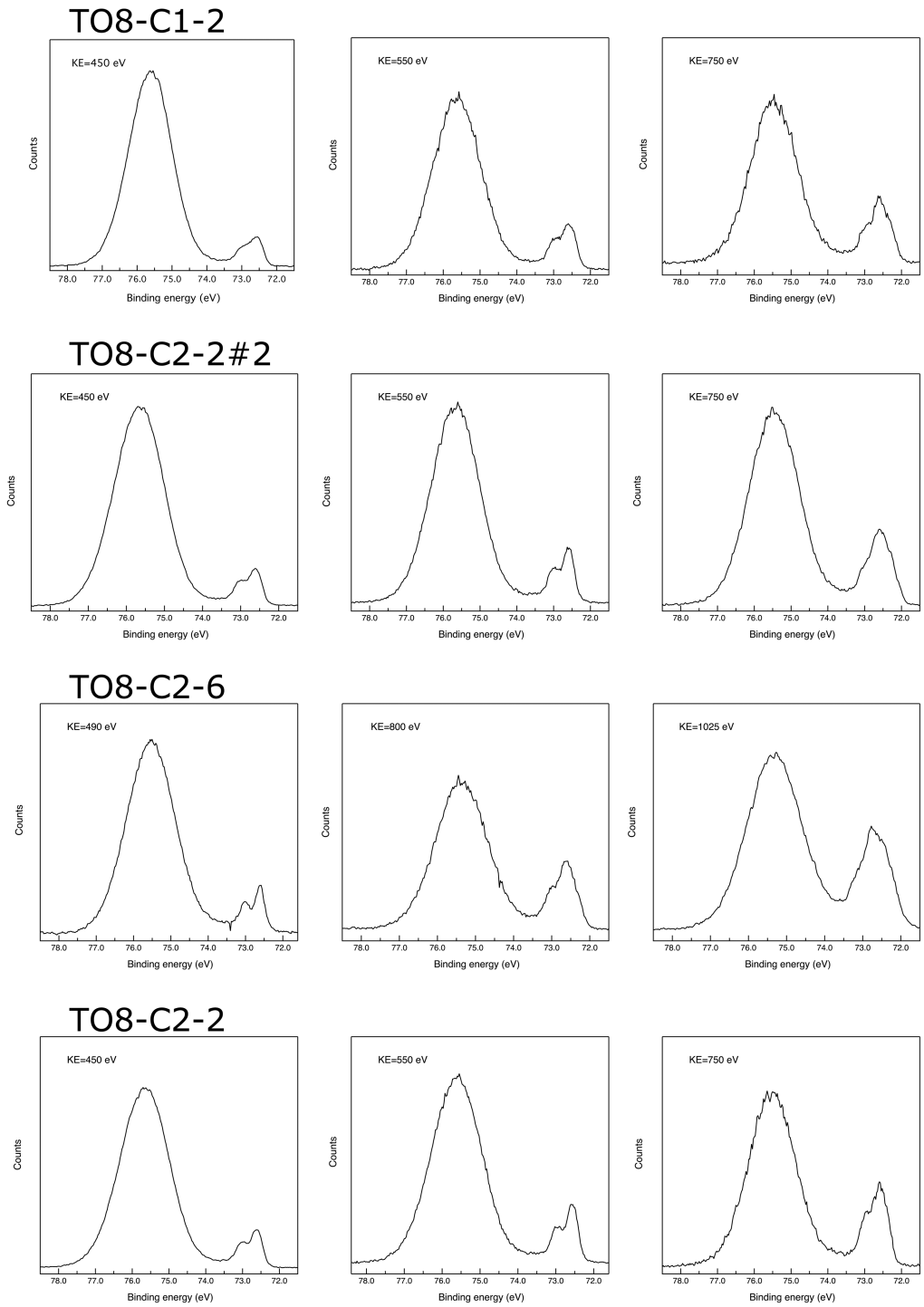

Fig. 3 Al 2p spectra of the TO8-C1-2 (first row), TO8-C2-2#2 (second row), TO8-C2-6 (third row), and TO8-C2-2 (fourth row) samples at different kinetic energies (KE) of the outgoing electrons. The specific KE is reported inside each plot.

Assuming a flat homogeneous oxide layer on top of a homogenous Al substrate, the thickness of the aluminum oxide, t, can be calculated using the following equation:[17]

$$t = \lambda_o \cos \alpha \ln(Q + 1), \tag{1}$$

where λ_o is the EAL of analyzed photoelectrons in the aluminum oxide, α the detection angle with respect to the surface normal, and Q is reported in the following equation:

$$Q = \frac{I_o}{I_m} * \frac{N_m}{N_o} * \frac{\lambda_m}{\lambda_o}, \tag{2}$$

where I_o and I_m are the areas (obtained by fitting procedure) of Al 2p components of the oxide and the metal, respectively, N_o and N_m are the atomic density (number of atoms per unit volume) of Al in the oxide and the metal, respectively, and λ_m is the EAL for the metallic aluminum.

The EALs are computed using the NIST EAL database[18] and the TPP- 2M predictive formula.[19] The values of the photoionization asymmetry parameter were taken from Ref. 20. The uncertainties of the EAL are considered for Al and Al_2O_3 10.9 and 17.4 % is considered, respectively.[18]

For the Al_2O_3 overlayer, we assume the density of 3.3 g cm^{-3}, band gap energy 7.0 eV[21] and 24 valence electrons per molecule. The ratio between the atomic densities was set at 1.5 and the areas of the Al 2p components were obtained by fitting the Al 2p peaks. An example of peak analysis is reported in Fig. 4.

The oxide thickness is calculated as the slope of the linear fit of Eq. (3), reported in Fig. 5

$$\lambda_o = t \frac{1}{\cos\,\alpha\,\ln(Q+1)}. \tag{3}$$

The oxide thicknesses computed for all analyzed spectra are reported in Table 6.

Such values are in good agreement with the thickness of native oxide on bulk Al(111) and Al(100) crystals[16] and with the oxide thickness that was found in witness samples of the current baseline filters for the Athena X-ray integral field unit and WFI detectors,[22] while it is very different to the case of the XMM back-up filters monitored over time.[23] In the last case, the aluminum oxide thickness was found to be 5.9 nm, thus nearly twice that measured for the samples investigated in this paper.

The main purpose of the X-ray transmission measurements performed at BESSY II was to model the transmission curve of each filter, derive the areal density ρx of the filter material and the thickness of each layer, with its associated uncertainties. Two fit functions were used, one involving the single atoms (elements) and disregarding the stoichiometry,[24] and the other using the chemical formula of each layer of the filter material.

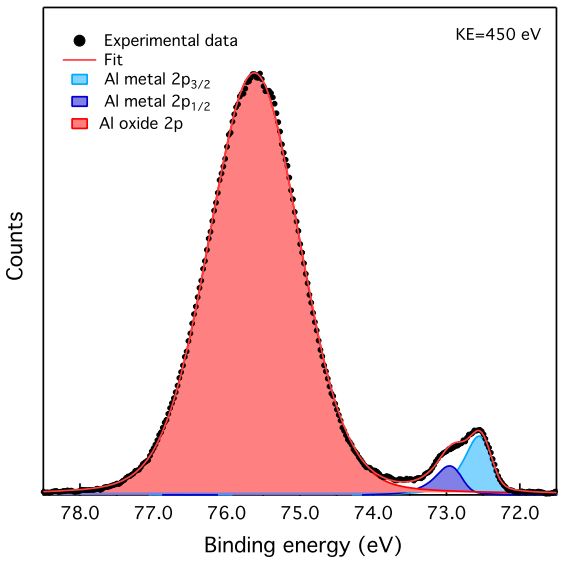

Fig. 4 XPS scan of the Al 2p peak at KE of 450 eV of the TO8-C1-2 sample. Data reported are experimental (black circles), best fit (red solid line), Al oxide 2p component (red filled curve) Al metal 2p1/2 (dark blue filled curve), and Al metal 2p3/2 (light blue filled curve).

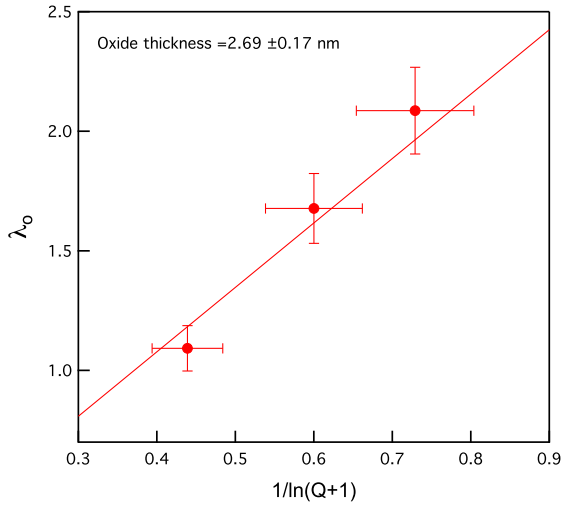

Fig. 5 Plot of λ_o versus the inverse of the logarithm of Eq. (1) (red circles) and linear fit (red line).

Table 6 Oxide thicknesses obtained from XPS analysis of the Al 2p peak for the TO8-C1-2, TO8-C2-2#2, TO8-C2-6, and TO8-C2-2 samples.

Sample name	Oxide thickness (nm)
TO8-C1-2	2.97 ± 0.19
TO8-C2-2#2	2.85 ± 0.18
TO8-C2-6	2.69 ± 0.17
TO8-C2-2	2.86 ± 0.18

The fit using elements has up to four parameters, namely each atomic areal density $\rho x_{i\text{-th}}$

$$T(E)_{\text{filter elements}} = T_{Al} * T_{Si} * T_O * T_N = e^{\left[-\frac{\mu}{\rho}(E)*\rho x\right]_{Al}} * e^{\left[-\frac{\mu}{\rho}(E)*\rho x\right]_{Si}} * e^{\left[-\frac{\mu}{\rho}(E)*\rho x\right]_O} * e^{\left[-\frac{\mu}{\rho}(E)*\rho x\right]_N}. \quad (4)$$

The fit function is based on the product of the transmission due to the i-th element T_i, and has four free parameters, the areal density ρx_i of each element. The quantity μ/ρ is the mass attenuation coefficient of the i'th chemical element and is calculated from the atomic scattering factors by Henke et al.[25] Hydrogen was not included since it does not contribute to the transmission of the filter in the investigated energy range. In principle, all layer thicknesses can be estimated, introducing two quantities *a posteriori*: material density and stoichiometry [see Eqs. (5) and (6)]. From ρx_{Al} one can approximately calculate the thickness of the Al layer by dividing it for the Al bulk density of 2.7 g/cm^3 (in so doing, one considers only the aluminum in bulk form). To estimate the silicon nitride thickness, one can calculate the equivalent thickness, x_N within the SiN_y using a stoichiometry $y = 4/3$

$$x_N = \frac{\rho x_N}{\rho_{\text{SiN}_y} f_N}, \quad (5)$$

where ρ_{SiNy} is the silicon nitride density and

$$f_N = \frac{yA_N}{yA_N + A_{Si}}, \quad (6)$$

is the fraction of mass of nitrogen within the silicon nitride molecule, which is 0.399, calculated by dividing the total mass of N by the silicon nitride relative molecular mass.

The fit using materials has up to three parameters, namely each material thickness

$$T(E)_{\text{filter materials}} = e^{\left[-\frac{\mu}{\rho}(E)*\rho x\right]_{\text{Al}}} * e^{\left[-\frac{\mu}{\rho}(E)*\rho x\right]_{\text{Al}_2\text{O}_3}} * e^{\left[-\frac{\mu}{\rho}(E)*\rho x\right]_{\text{Si}_3\text{N}_4}}. \quad (7)$$

The second material is a layer of aluminum oxide, whose presence is a well-established fact in the literature and is proven by the XPS measurements reported above. The advantage of using materials instead of atoms lies in that it is possible to directly obtain each layer thickness (using the following densities: $\rho_{\text{Al}} = 2.7$ g/cm^3, $\rho_{\text{Al2O3}} = 3.3$ g/cm^3, and $\rho_{\text{Si3N4}} = 3.44$ g/cm^3) and make a comparison with the nominal thicknesses. A correction needs to be introduced for the filters supported by a mesh, to consider the OA and the mesh material, which is not generally opaque and could be transparent to X-rays at the higher end of the investigated energy spectrum. To this end, two more parameters were considered, namely the mesh material areal density and the OA, as seen by the beam spot (which is generally different from the nominal value)

$$\text{T(E)}_{\text{filter+mesh}} = T(E)_{\text{filter}} \left[OA + (1 - OA) * e^{\left[-\frac{\mu}{\rho}(E)*\rho x\right]_{Si\,mesh}}\right]. \quad (8)$$

Two best fits, one using elements and one using materials, were obtained for all the filter samples. For filters with a mesh, the additional parameters of mesh areal density and OA were derived. The areal densities and OA of the best fit on elements and the derived thicknesses are summarized in Table 7, whilst the layer thicknesses, mesh thickness and OA obtained from the best fit on materials are reported in Table 8.

The measured X-ray transmission spectra of the investigated filters are shown in Figs. 6–10 along with the best fits and details at the absorption edges of the involved elements. In general, all fits are globally good, also at the Al, Si, and N edges, but discrepancies are visible at the O edges, partly related to the low amount of O.

As can be seen in Table 8, the sum of the Al and the Al_2O_3 thicknesses is in agreement, within the uncertainties, with the equivalent thicknesses of the Al layer, calculated from the areal densities in Table 7. In most cases, it is slightly higher than the nominal Al thickness. Furthermore, for the samples with the thin silicon nitride substrate, the Al_2O_3 thickness varies from sample to sample, probably due to the fit being less accurate around the O K-edge. The obtained thickness of the SiN substrate itself deviates only a few percent from the nominal values. The obtained OA from both fits is also close to the nominal value. Estimating the mesh thickness is trickier, because both the OA and the mesh areal density are interdependent parameters and difficult to disentangle for the optimization algorithm.

Transmission spectra acquired in the UV/VIS/NIR range are reported in Figs. 11 and 12. The reported spectra show that these filters are quite transparent in the UV region (190 to 400 nm), partly due to the constructive interference effects generated by the bilayer of aluminum, while in the visible portion of the spectra the rejection of the radiation is more efficient.

The shape of the transmission curves of Fig. 12 does not look affected by the irradiation treatment, suggesting that these multilayers are quite resistant when proton irradiation occurs. Although a blueshift of the main peak (close to 300 nm) must be noticed when the Q.F. increases,

Table 7 Areal densities of each element (Al, Si, O, N, and Si mesh) and OA with 3σ statistical uncertainty.

Sample name	Areal densities (10^{-7} g/cm^2)				Si mesh thickness (μm)	OA (%)	Al equivalent thickness (nm)	SiN equivalent thickness (nm)
	Al	Si	O	N				
TO8-C1-1	54 ± 2	280 ± 3	0 ± 3	205 ± 3	—	—	20 ± 1	149 ± 2
TO8-C2-6	94 ± 2	75 ± 2	18 ± 2	67 ± 2	34 ± 2	84 ± 1	35 ± 1	48 ± 2
TO8-C2-5	89 ± 1	74 ± 1	8 ± 1	60 ± 1	32 ± 1	84 ± 1	33 ± 1	44 ± 2
TO8-C2-2	92 ± 2	70 ± 2	22 ± 2	59 ± 2	32 ± 2	83 ± 1	34 ± 1	43 ± 2
TO8-C2-31	—	79 ± 1	0 ± 1	56 ± 2	32 ± 2	82 ± 1	—	41 ± 2

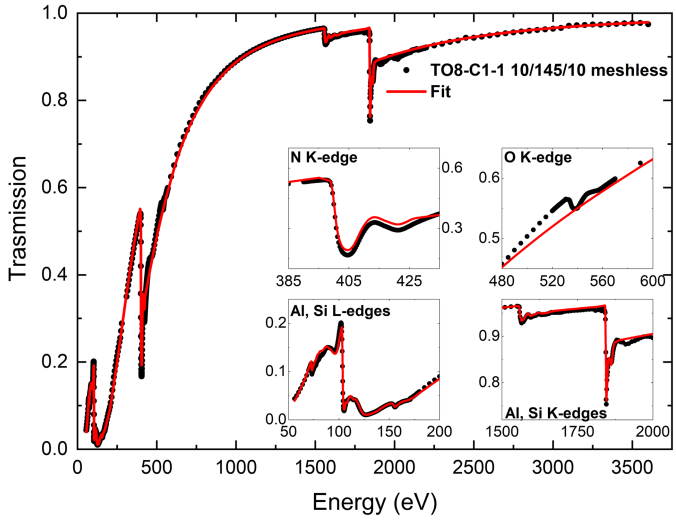

Fig. 6 Experimental data (black points) of TO8-C1-1 filter and the best fit on elements (red line).

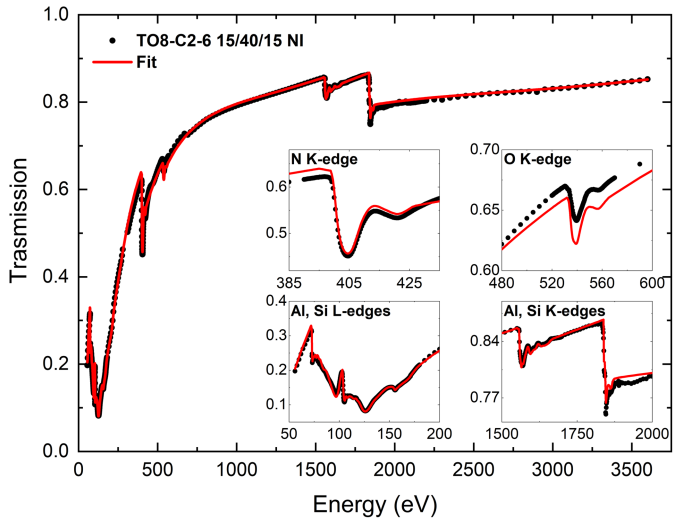

Fig. 7 Experimental data (black points) of TO8-C2-6 filter and the best fit on elements (red line).

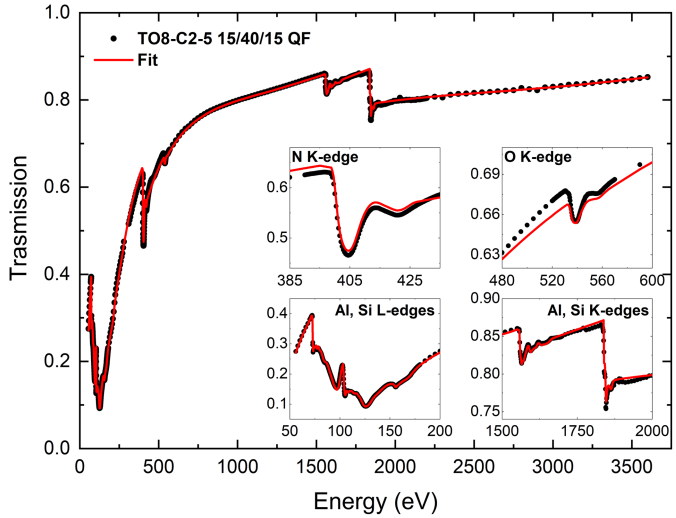

Fig. 8 Experimental data (black points) of TO8-C2-5 filter and the best fit on elements (red line).

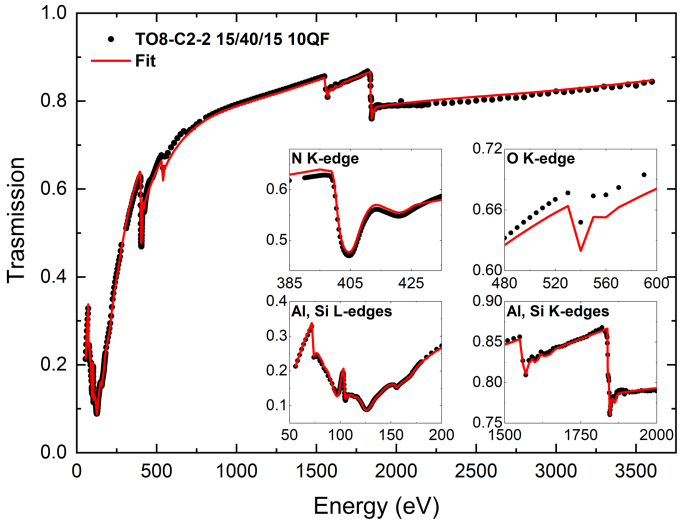

Fig. 9 Experimental data (black points) of TO8-C2-2 filter and the best fit on elements (red line).

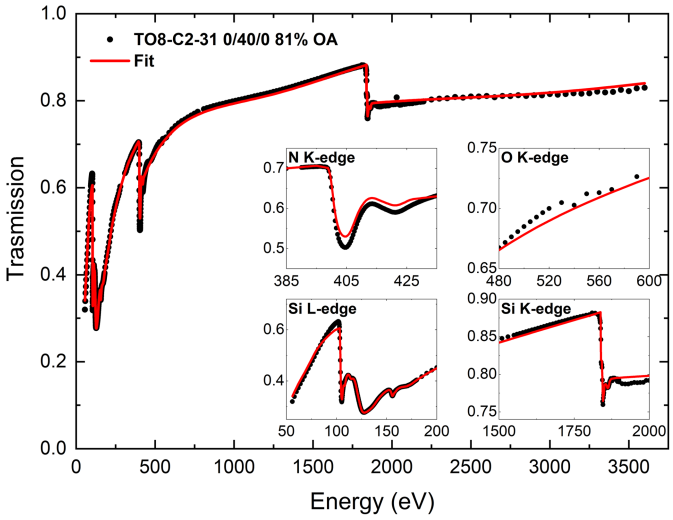

Fig. 10 Experimental data (black points) of TO8-C2-31 filter and the best fit on elements (red line).

Table 8 Layer thickness of each material (Al, Al_2O_3, SiN, SiO_2, and Si mesh) and OA with 3σ statistical uncertainty and nominal thickness for all filters.

	Best fit thicknesses					Nominal thicknesses			(%)
Sample name	Al (nm)	SiN (nm)	Al_2O_3 (nm)	Si mesh (μm)	OA (%)	Al (nm)	SiN (nm)	Si mesh (μm)	OA
TO8-C1-1	18 ± 2	142 ± 1	3.0 ± 1	—	—	2 × 10	145	—	—
TO8-C2-6	22 ± 1	41 ± 1	17 ± 1	15 ± 1	84 ± 1	2 × 15	40	15	82
TO8-C2-5	26 ± 1	39 ± 1	8 ± 1	14±	83 ± 1	2 × 15	40	15	82
TO8-C2-2	21 ± 1	37 ± 1	18 ± 1	13 ± 1	83 ± 1	2 × 15	40	15	82
TO8-C2-31	—	39 ± 1	—	13 ± 1	82 ± 1	—	40	15	81

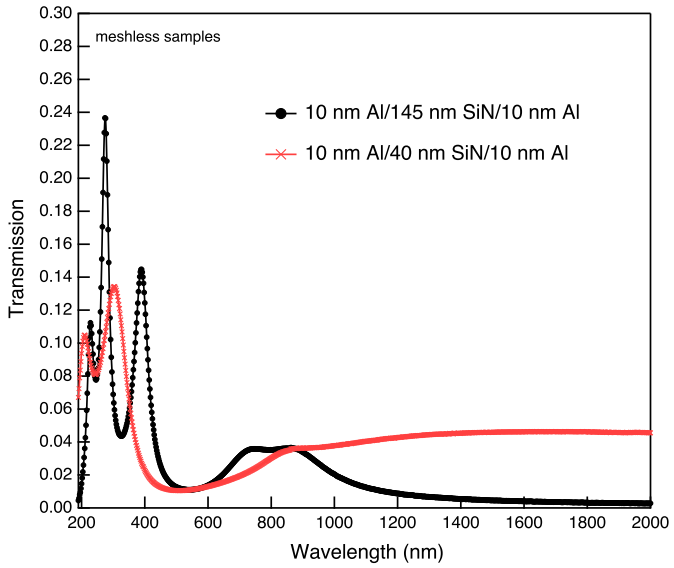

Fig. 11 UV/VIS/NIR transmission of meshless samples the TO8-C1-1 (black line) and TO8-C2-1#2 (red line).

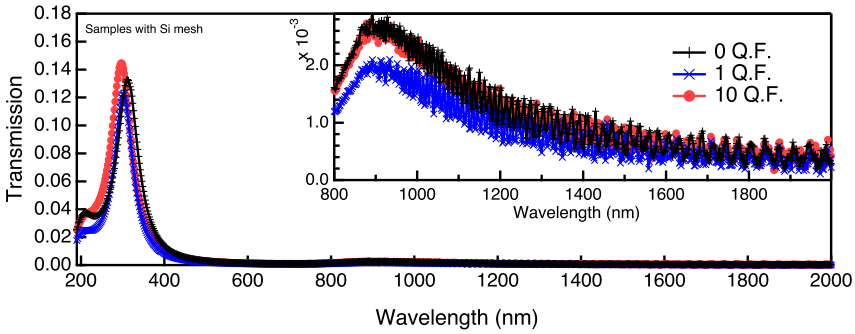

Fig. 12 UV/VIS/NIR transmission of samples with meshes with different proton irradiation doses, namely: the TO8-C2-6 (0 Q.F. black line), the TO8-C2-5 (1 Q.F. blue line), and TO8-C2-2 (10 Q.F. red line).

this peak moves from 312 nm (pristine filter, 3.97 eV) to 302 nm (1 Q.F. sample, 4.11 eV) and to 296 nm (10 Q.F., 4.19 eV).

Zhang et al. showed that the position of the aluminum absorption band close to 4 eV is size-dependent: if the size of the nanoparticle increases, the peak redshifts.[26] Then the observed blue-shift in our work might be ascribed to a slight reduction of the size of aluminum nanoparticles assembled to create the metal coating.

AFM images were analyzed using the data analysis software Gwyddion[27] and are reported in Fig. 13. The zero-height reference is located in the lowest point measured by the probe.

Since in literature it is found that ion irradiation can affect the aluminum surface[28,29] and that proton irradiation may create ripples and hillocks changing the roughness of the surfaces,[30] both the roughness and the average heights are computed.

The roughness, R, of the samples was calculated as reported in the following equation:

$$R = \sqrt{\frac{1}{N}\sum_{j=1}^{N} r_j^2}, \tag{9}$$

where r_j is the difference between the height and the average height of the j'th measurement. The calculated roughness for the samples TO8-C2-1, TO8-C2-6, and TO8-C2-3 are 1.95 nm,

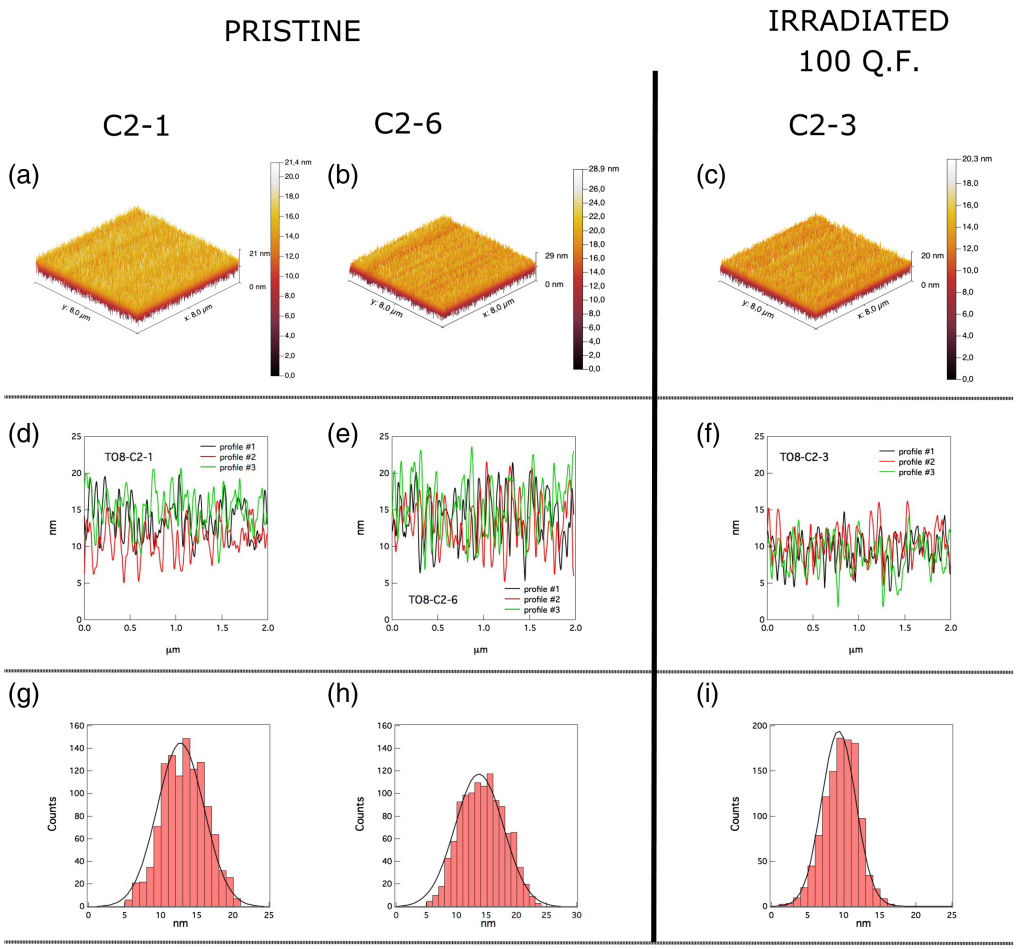

Fig. 13 AFM data and analysis. (a)–(b) The 3D images of the upper images of the TO8-C2-1, TO8-C2-6, and TO8-C2-3, respectively. (d)–(f) Typical height profiles of the TO8-C2-1, TO8-C2-6, and TO8-C2-3, respectively. (g)–(i) The histograms of the above height profiles (red columns) and the fit (black line) of the TO8-C2-1, TO8-C2-6, and TO8-C2-3, respectively.

3.56 nm, and 2.39 nm, respectively. Among these samples, only the sample TO8-C2-3 has been irradiated; we can conclude that the roughness is not significantly affected by irradiation.

The height data, obtained from the z-profiles [Figs. 13(d)–13(f)], are reported in three histogram plots [Figs. 13(g)–13(i)], and fitted using a Gaussian curve. The average heights correspond to the maxima of the fits. The obtained average heights for the samples TO8-C2-1, TO8-C2-6, and TO8-C2-3 are 12.75 nm, 13.78 nm, and 9.32 nm, respectively. The AFM analysis suggests that the average heights of the pristine samples are larger than the irradiated filter, this may hint at the possibility of an erosion process due to the proton exposure as suggested by Sznajder et al.[31]

4 Conclusions

The analyses of the XPS spectra we reported show that Al/SiN/Al is undoubtedly oxidized on the surface. The thickness values that we find for the surface oxide agree with other results, already reported in the literature, for Al-coated polymeric filters.[20,21] The irradiation treatment has no relevant effect on the surface oxide thickness up to 10 Q.F. On the other hand, the amount of oxide revealed by the X-ray transmission measurement is larger than the one obtained by XPS, because this technique is sensitive to the bulk, consequently, the whole amount of the present aluminum oxide is detected: both the two layers on the two external coating surfaces and any interfacial Al oxide between the silicon nitride and the aluminum coating. Moreover, the amount of Al oxide computed by the X-ray transmission model might be affected by the presence of Si_xO_y, which can be found on the silicon mesh and/or the silicon nitride.

Both surface roughness and UV/VIS/NIR transmission are not significantly affected by proton irradiation. The samples we studied are rather transparent below 400 nm; this can be ascribed to a total small amount of aluminum (20 nm) of which at least 20% is oxidized. To design an effective OBF for use in high energy astrophysical space missions based on SiN, the amount of Al must be increased to at least 30 nm possibly deposited on a single side to reduce the aluminum oxidation. However, this choice would cause a low transmission in the soft X-rays, that for the investigated samples is already <70% at 0.5 keV. These materials can be proposed in those cases where the presence of carbon atoms might be an issue although the capability to manufacture very thin large area membranes and their mechanical performances under differential pressure and dynamic launch stresses needs to be demonstrated.

Disclosures

The authors have no financial interests in the manuscript and no other potential conflicts of interest to disclose.

Code and Data Availability

The data that support the findings of this article are not publicly available due to privacy. They can be requested from the author at luisa.sciortino@inaf.it.

Acknowledgments

We acknowledge Elettra Sincrotrone Trieste for providing access to its synchrotron radiation facilities and for financial support, we received the Italian full support for both the proposals (Grant Nos. 20180369 and 20190214). E.M., S.N., and I.P. acknowledge funding from EUROFEL project (RoadMap ESFRI). The research leading to these results received funding from the European Space Agency for the project "Large Area high-performance Optical Filters for X-ray instrumentation – LAOF" (Grant No. 4000120250/17/NL/BJ), and from the European Union's Horizon 2020 Program for the project AHEAD2020 (Grant No. 871158).

References

1. N. Meidinger et al., "The wide field imager instrument for Athena," *Proc. SPIE* **10397**, 103970V (2017).
2. M. Barbera et al., "The optical blocking filter for the ATHENA wide field imager: ongoing activities towards the conceptual design," *Proc. SPIE* **9601**, 960109 (2015).
3. L. Golub et al., "The X-ray telescope (XRT) for the Hinode mission," in *The Hinode Mission*, T. Sakurai, Ed., Springer, New York, NY (2008).
4. J.-P. Delaboudinière et al., "EIT: Extreme-ultraviolet Imaging Telescope for the SOHO mission," *Sol. Phys.* **162**, 291–312 (1995).
5. P. Rochus et al. "The solar orbiter EUI instrument: the extreme ultraviolet imager," *Astron. Astrophys.* **642**, A8 (2023).
6. P. T. Törmä et al., "Ultra-thin silicon nitride x-ray windows," *IEEE Trans. Nucl. Sci.* **60**(2), 1311–1314 (2013).
7. P. T. Törmä et al., "Performance and properties of ultra-thin silicon nitride x-ray windows," *IEEE Trans. Nucl. Sci.* **61**(1), 695–699 (2014).
8. M. Tatarková, P. Tatarko, and P. Šajgalík, "Si_3N_4 ceramics, structure and properties," in *Encyclopedia of Materials: Technical Ceramics and Glasses*, pp. 109–118, Elsevier (2020).
9. https://www.jedec.org/standards-documents/focus/registered-outlines-jep95/transistor-outlines-archive.
10. M. Barbera et al., "Athena WFI optical blocking filters development status toward the end of the instrument phase-A," *Proc. SPIE* **10699**, 106991K (2018).
11. M. Barbera et al., "ATHENA X-IFU thermal filters development status toward the end of the instrument phase-A," *Proc. SPIE* **10699**, 106991R (2018).
12. R. Amato et al., "Scattering efficiencies measurements of soft protons at grazing incidence from an Athena silicon pore optics sample," *Exp. Astron.* **52**, 109–123 (2021).
13. M. Schmid, H. P. Steinrück, and J. M. Gottfried, "A new asymmetric Pseudo-Voigt function for more efficient fitting of XPS lines," *Surf. Interface Anal.* **46**(8), 505–511 (2014).
14. F. Scholze et al., "High-accuracy EUV metrology of PTB using synchrotron radiation," *Proc. SPIE* **4344**, 402–413 (2001).
15. M. Krumrey and G. Ulm, "High-accuracy detector calibration at the PTB four-crystal monochromator beamline," *Nucl. Instrum. Method A* **467–468**, 1175–1178 (2001).

16. J. Evertsson et al., "The thickness of native oxides on aluminum alloys and single crystals," *Appl. Surf. Sci.* **349**, 826–832 (2015).
17. A. Jablonski, "Evaluation of procedures for overlayer thickness determination from XPS intensities," *Surf. Sci.* **688**, 14–24 (2019).
18. C. J. Powell and A. Jablonski, *NIST Electron Effective-Attenuation-Length Database – Version 1.3*, National Institute of Standards and Technology, Gaithersburg, MD (2011).
19. S. Tanuma, C. J. Powell, and D. R. Penn, "Calculations of electron inelastic mean free paths," *Surf. Interface Anal.* **21**, 165 (1994).
20. J. J. Yeh and I. Lindau, "Atomic subshell photoionization cross section and asymmetry parameters: $1 \leq Z \leq 103$," *Atomic Data Nucl. Data Tables* **32**, 1–155 (1985).
21. E. O. Filatova and A. S. Konashuk, "Interpretation of the changing the band gap of Al_2O_3 depending on its crystalline form: connection with different local symmetries," *J. Phys. Chem. C* **119**(35), 20755–20761 (2015).
22. L. Sciortino et al., "Surface investigation and aluminum oxide estimation on test filters for the ATHENA X-IFU and WFI detectors," *Proc. SPIE* **9905**, 990566 (2016).
23. M. Barbera et al., "The thin and medium filters of the EPIC camera on-board XMM-Newton: measured performance after more than 15 years of operation," *Exp. Astron.* **42**, 179–197 (2016).
24. E. Puccio et al., "Synchrotron x-ray transmission measurements and modeling of filters investigated for Athena," *J. Astron. Telesc. Instrum. Syst.* **6**(3), 038003 (2020).
25. B. L. Henke et al., "X-ray interactions: photoabsorption, scattering, transmission, and reflection at E. 50 − 30; 000 eV, Z. 1 − 92," *Atomic Data Nucl. Data Tables* **54**, 181–342 (1993).
26. P. Zhang, W. Jin, and W. Liang, "Size-dependent optical properties of aluminum nanoparticles: from classical to quantum description," *J. Phys. Chem. C* **122**, 10545–10551 (2018).
27. D. Nečas and P. Klapetek, "Gwyddion: an open-source software for SPM data analysis," *Cent. Eur. J. Phys.* **10**(1), 181–188 (2012).
28. K. Dae-Weon et al., "Influence of MeV protons on mechanical properties of ITO/aluminum-coated Kapton designed for space missions," *Nucl. Instrum. Methods Phys. Res. B* **266**, 3263–3274 (2008).
29. M. Sznajder, U. Geppert, and M. Dudek, "Degradation of metallic surfaces under space conditions, with particular emphasis on hydrogen recombination processes," *Adv. Space Res.* **56**(1), 71–84 (2015).
30. W. Qiang et al., "Characterization of surface morphology changes induced by proton irradiation of an aluminum film reflector," *AIP Conf. Proc.* **1087**, 657 (2009).
31. M. Sznajder, U. Geppert, and M. R. Dudek, "Hydrogen blistering under extreme radiation conditions," *NPJ Mater. Degrad.* **2**, 3 (2018).

Luisa Sciortino (PhD in chemistry, Italy, in 2012) is a permanent staff member of the INAF-OAPA, Palermo, Italy. She has been working on the development of thermal and optical blocking filters for high-energy astrophysical mission. Her interest is focused on the spectroscopic and morphological characterization of materials.

Biographies of the other authors are not available.